Localized plastic deformation in ternary polymer blends

Seelig, T.; van der Giessen, E.

Published in:
International Journal of Solids and Structures

DOI:
10.1016/S0020-7683(02)00161-0

Publication date:
2002

PERGAMON

International Journal of Solids and Structures 39 (2002) 3505–3522

INTERNATIONAL JOURNAL OF SOLIDS and STRUCTURES

www.elsevier.com/locate/ijsolstr

Localized plastic deformation in ternary polymer blends

Th. Seelig [a,*], E. van der Giessen [b]

[a] *Institute of Mechanics, TU Darmstadt, Hochschulstrasse 1, D-64289 Darmstadt, Germany*
[b] *Micromechanics of Materials Group, University of Groningen, 9747 AG Groningen, The Netherlands*

Received 13 February 2002

Abstract

Patterns of localized plastic strain in polycarbonate (PC)/acrylonitrile–butadiene–styrene (ABS) polymer blends are investigated numerically with respect to their dependence on the blend microstructure as well as their interrelation to toughening mechanisms in these materials. Modeling of the blends consists of two steps: the representation as a two-phase material of ABS particles embedded in a PC matrix and the development of a homogenized constitutive description of ABS which itself has a heterogeneous microstructure. The constitutive models for the two phases account for large visco-plastic strains, the intrinsic softening-rehardening behavior of glassy polymers as well as plastic dilatation in the ABS phase to comprise the effect of rubber particle cavitation.

Cell model calculations for periodic microstructures illustrate that patterns of localized plastic deformation in the blend are qualitatively different for different ABS modifier types. Network-like shear banding in the PC matrix is found to be beneficial for toughening by reducing peak hydrostatic stresses. Quantitative analyzes indicate that toughening in PC/ABS blends may be most efficient for a rubber content in ABS in an intermediate range of 5–35%.

Keywords: Polymer blends; Shear banding; Rubber cavitation; Plastic dilatancy; Toughening mechanisms

1. Introduction

A large number of experimental investigations have shown that the fracture toughness of amorphous polymers can be improved by blending these materials with a second, mostly rubbery phase (e.g. Yee, 1977; Bucknall, 1997). Although the detailed mechanisms differ with the material combination, it is a common feature that the modifier phase serves to promote inelastic deformations in the thermoplastic matrix leading to an enhanced energy absorption. The inelastic deformation behavior of amorphous thermoplastic polymers, such as for example polycarbonate (PC), displays a distinctly different phenomenology than that of metals because of the macromolecular structure of these materials (e.g. Boyce et al., 1988; G'Sell et al.,

* Corresponding author. Tel.: +49-6151-16-4648; fax: +49-6151-16-3018.
E-mail address: seelig@mechanik.tu-darmstadt.de (Th. Seelig).

0020-7683/02/$ - see front matter
PII: S0020-7683(02)00161-0

1992). Intrinsic softening after the onset of yield gives rise to localization of the deformation by shear banding or necking. In contrast to metals this need not be a precursor of failure, but is stabilized by progressive rehardening of the material due to alignment of the macromolecular network at large stretches. In spite of this, neat PC and other unmodified plastics show a severe notch sensitivity and may fail in a brittle manner by crazing, which is initiated essentially by the high hydrostatic stresses prevailing at notches and crack tips (e.g. Donald, 1997). When PC is blended with small rubber particles of submicron size, cavitation of these rubber particles facilitates plastic 'shear yielding' in the surrounding matrix material and at the same time delays or suppresses crazing by the relief of hydrostatic stress. Another prominent example is acrylonitrile–butadiene–styrene (ABS) where toughening is also due to enhanced energy dissipation in the SAN (styrene–acrylonitrile) matrix promoted by rubber (butadiene) particle cavitation.

In recent years PC/ABS 'ternary' blends (ternary because ABS itself is a blend of SAN and rubber particles) have become a frequently used engineering material combining several advantageous properties of both components. From the relatively small number of experimental works on PC/ABS blends (Greco et al., 1994; Ishikawa, 1995; Greco, 1996; Inberg, 2001), the toughening effect is again attributed to rubber particle cavitation in the ABS phase and enhancement of plastic yielding in the PC matrix. However, in contrast to 'binary' blends such as PC/rubber or ABS, the detailed mechanisms are far less well understood. This is partly due to the enriched set of parameters, of which—from a mechanics point of view—the most important ones are the ABS composition (rubber content), the ABS content in the PC/ABS blend and the morphology which itself may vary with the blend composition. Experiments show a correlation between these parameters, the amount of micro-plastic deformations visible on the fracture surface and the 'resulting' fracture toughness (Greco et al., 1994). It is the aim of the present work to gain some basic insight into the role of localized plastic deformations in ternary (PC/ABS) blends in the process of toughening and how this depends on parameters characterizing the blend microstructure.

Numerical studies taking into account the large strain visco-plastic softening and rehardening behavior of glassy polymers have so far focused on rubber modified binary blends. A usually made convenient assumption for these materials is to approximate the soft and cavitating rubber particles as voids. Unit cell models for periodic arrays of voids have been employed to investigate the evolution of shear band patterns in the thermoplastic matrix during void growth under various stress triaxialities (Steenbrink et al., 1998) or during macroscopic shearing as experienced by blends in the neighborhood of a moving crack tip (Pijnenburg et al., 1999). Three-dimensional (3D) unit cell calculations for porous PC were performed by Socrate and Boyce (2000) who also analyzed toughening implications in terms of peak values of hydrostatic stress in the matrix material. Smit et al. (1999) investigated large samples of porous PC with a random void arrangement where—in contrast to periodic void arrays—localization of plastic deformation occurs not only due to intrinsic matrix softening but also in form of bands of unstably growing voids percolating throughout the whole sample. Incorporating a realistic constitutive model for rubber, Steenbrink and Van der Giessen (1999) addressed the process of rubber cavitation and analyzed the influence of the rubber properties on the overall yield behavior.

In the present work, ternary blends of PC/ABS are modeled as a two-phase material by homogenizing the ABS microstructure (Section 2). Applying the approximation of cavitated rubber particles as voids to the ABS phase, we describe ABS by the overall behavior of porous SAN. An appropriate constitutive model allowing for volumetric yielding is developed in Section 3.2 after briefly summarizing the equations representing homogeneous glassy polymers (PC, SAN) in Section 3.1. Employing 2D unit cell models of the PC/ABS blend microstructure, we investigate patterns of localized plastic deformation—now enriched by those arising from volumetric softening in the ABS phase—in Section 4.1. Qualitative differences in shear band patterns in the PC matrix are shown to depend strongly on the ABS behavior. Quantitative effects of the blend composition on the overall toughness—traced in terms of energy absorption and hydrostatic stress—are analyzed in Section 4.2. Conclusions to be drawn from these results, e.g. with respect to an optimal blend composition, are discussed in the light of experimental observations.

2. Formulation of the blend model

In order to investigate deformation mechanisms on the PC/ABS blend level and their toughening implications, the blend microstructure is modeled as a two-phase material of ABS particles embedded in a PC matrix. The even finer microstructure of ABS consisting of rubber particles in a SAN matrix (Fig. 1) is not explicitly accounted for but treated in a homogenized sense. After having cavitated, the rubber particles are regarded mechanically equivalent to voids and ABS is represented by the overall behavior of porous SAN as will be described in Section 3.2. In the range of ABS volume fractions up to about 40%, the ABS particles are found to be approximately spherical with a diameter of a few microns (Greco et al., 1994). Since the particles are much smaller than the initial notch radius of 0.1–1 mm in typical fracture test specimens (e.g. Ishikawa, 1995; Inberg, 2001), we consider a 'representative volume element' (RVE) of the blend material to be subjected to states of uniform macroscopic loading (Fig. 1). As a consequence all length scales are eliminated, and the only microstructural parameters entering the model are the ABS volume fraction and the rubber content (i.e. porosity) in ABS.

In the present 2D plane strain model, the ABS particles are in fact cylinders in the third direction. By idealizing the blend microstructure as a square or hexagonal array of particles, only a unit cell of the periodic arrangement needs to be considered in the analysis (Fig. 2a). With the principal directions of macroscopic deformation taken to coincide with symmetry axes of the blend model, it follows that the unit

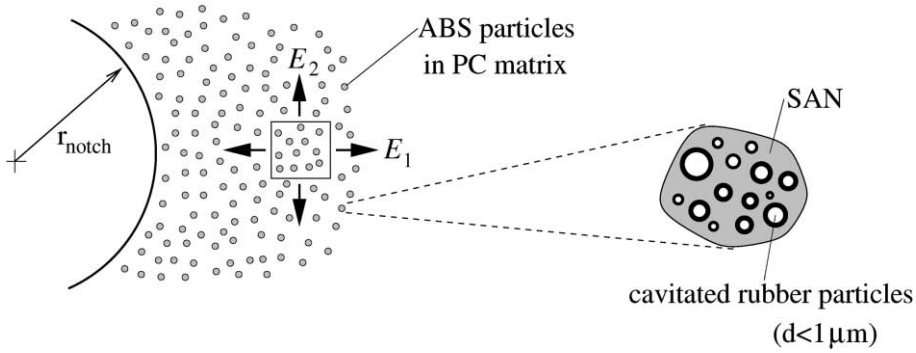

Fig. 1. Modeling PC/ABS ('ternary') blends.

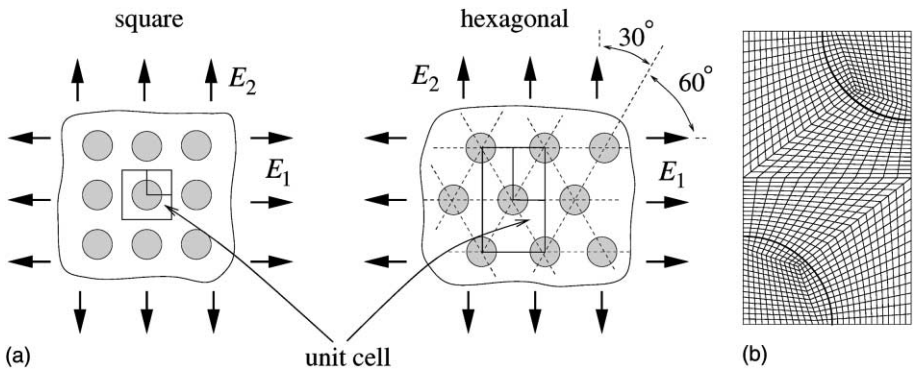

Fig. 2. (a) Periodic 2D microstructures of ABS particles in PC matrix. (b) FE mesh of hexagonal unit cell exploiting symmetry of loading.

cell boundaries remain straight during deformation and the periodic boundary conditions simplify to constant normal displacements and vanishing shear tractions on each side of the cells. Loading of the blend material is specified in terms of principal logarithmic strains $E_1 = \ln U_1$ and $E_2 = \ln U_2$ (Fig. 1) where U_i are the macroscopic principal stretches. For a given strain ratio E_2/E_1, a constant rate of deformation $\dot{U}_1$ is specified by prescribing the values of the normal velocities on the cell boundaries. Due to symmetry the analysis can be reduced to a quarter of the cells depicted in Fig. 2a; the finite element mesh for the hexagonal case is shown in Fig. 2b. The macroscopic true stress $\boldsymbol{\Sigma}$ acting on the blend material is defined as the volume average of the Cauchy stress $\boldsymbol{\sigma}$. Different macroscopic strain ratios E_2/E_1 will lead to different macroscopic stress triaxialities $T_\Sigma = \Sigma_m/\Sigma_e$ where Σ_m and Σ_e are the macroscopic mean and Mises stress, respectively. For plane strain conditions, they can be approximated by $\Sigma_m = (\Sigma_1 + \Sigma_2)/2$ and $\Sigma_e = |\Sigma_1 - \Sigma_2|\sqrt{3}/2$ with principal macrostresses Σ_1 and Σ_2.

3. Constitutive equations

3.1. Matrix behavior—homogeneous glassy polymer

The constitutive model for the large strain visco-plastic behavior of amorphous polymers has originally been derived by Boyce et al. (1988) and in the present work follows exactly the modified version given in Wu and Van der Giessen (1996). Here it captures the behavior of the PC matrix on the blend level as well as the SAN matrix in the ABS model (Section 3.2) with different sets of material parameters as listed in Table 1. It makes use of the standard additive decomposition of the rate of deformation tensor into its elastic and plastic parts: $\boldsymbol{D} = \boldsymbol{D}^e + \boldsymbol{D}^p$. Visco-elastic effects prior to yield are of minor importance in the present study and are neglected. The small strain elastic response is governed by Hooke's law written in rate form as

$$\boldsymbol{D}^e = \mathscr{L}^{-1}\overset{\triangledown}{\boldsymbol{\sigma}}, \tag{1}$$

where $\overset{\triangledown}{\boldsymbol{\sigma}}$ is the Jaumann rate of the Cauchy stress and $\mathscr{L}$ is the standard fourth-order isotropic elasticity tensor. The isochoric visco-plastic strain rate

$$\boldsymbol{D}^p = \frac{\dot{\gamma}^p}{\sqrt{2}\tau}\bar{\boldsymbol{\sigma}}' \tag{2}$$

is specified in terms of the equivalent plastic shear strain rate $\dot{\gamma}^p = \sqrt{\boldsymbol{D}^p \cdot \boldsymbol{D}^p}$ and the deviatoric driving stress $\bar{\boldsymbol{\sigma}}'$ normalized by the equivalent driving shear stress $\tau = (\frac{1}{2}\bar{\boldsymbol{\sigma}}' \cdot \bar{\boldsymbol{\sigma}}')^{1/2}$. The latter serves to determine $\dot{\gamma}^p$ via the visco-plastic constitutive equation

$$\dot{\gamma}^p = \dot{\gamma}_0 \exp\left[-\frac{A\tilde{s}}{T}\left(1 - \left(\frac{\tau}{\tilde{s}}\right)^{5/6}\right)\right], \tag{3}$$

where $\dot{\gamma}_0$ and A are material parameters, and T is the absolute temperature which is constant in the present analysis. The shear resistance $\tilde{s}$ is taken to evolve with plastic strain according to

$$\tilde{s}(\gamma^p) = s_s + (s_0 - s_s)\exp(-h\gamma^p/s_s) + \alpha p \tag{4}$$

Table 1
Material parameters used for PC and SAN in the present study

	E/s_0	ν	s_s/s_0	As_0/T	h/s_0	α	λ_{max}	C_R/s_0
PC	9.4	0.3	0.79	79.2	5.15	0.08	2.5	0.059
SAN	12.5	0.38	0.79	52.2	12.6	0.25	3.5	0.033

from an initial value s_0 to a saturation value s_s in order to phenomenologically model the intrinsic softening of the glassy polymer (Boyce et al., 1988). Furthermore, it incorporates (via a constant pre-factor α) the dependence of yield on the pressure $p = -\frac{1}{3}\mathrm{tr}\,\boldsymbol{\sigma}$. This pressure dependence is due to a changing molecular mobility and not associated with plastic dilatancy of the bulk material. From (2) and the definition of τ it follows that the plastic dissipation rate per unit volume of the material is given by $\bar{\boldsymbol{\sigma}}' \cdot \boldsymbol{D}^{\mathrm{p}} = \sqrt{2}\tau\dot{\gamma}^{\mathrm{p}}$. To elucidate the extension of the constitutive model to porous glassy polymers in the following section, it should be noted that the flow rule (2) can formally be obtained from

$$\boldsymbol{D}^{\mathrm{p}} = \lambda \frac{\partial \Phi}{\partial \bar{\boldsymbol{\sigma}}'}, \quad \text{where } \Phi = \frac{1}{2}\bar{\boldsymbol{\sigma}}' \cdot \bar{\boldsymbol{\sigma}}' - \tau^2. \tag{5}$$

The Mises-type yield function Φ then also defines the equivalent driving shear stress τ from the condition $\Phi = 0$ and the multiplier λ is determined from the expression for the plastic dissipation rate.

The progressive hardening of a glassy polymer after yield due to stretching of the molecular network is described by the back stress tensor $\boldsymbol{b}$ incorporated in the driving stress tensor $\bar{\boldsymbol{\sigma}}' = \boldsymbol{\sigma}' - \boldsymbol{b}$. Drawing on the analogy with cross-linked rubber (Arruda and Boyce, 1993) the principal components of the back stress tensor are—in an approximate manner—specified in terms of principal stretches. The back stress model involves two additional material parameters: the initial hardening modulus C_R and the limit stretch of the molecular chains $\lambda_{\max}$ at which the network responds with an infinite stiffness and no further yielding is possible. Full details of the constitutive model may be found in Wu and Van der Giessen (1996) along with a convenient numerical integration scheme.

3.2. Effective ABS behavior—porous glassy polymer

Once the rubber particles in the ABS phase have cavitated, they are considered mechanically equivalent to voids because of the low modulus of the rubber. The overall behavior of ABS can then be approximated by that of porous SAN. The SAN itself, being the thermoplastic matrix phase in ABS, is described by the constitutive model given in the previous section. The isotropic elasticity tensor for the porous material is now given in terms of effective elastic constants $E^*(f)$, $\nu^*(f)$, depending on the porosity f. Respective expressions obtained via the Mori–Tanaka scheme can be found e.g. in Pijnenburg and Van der Giessen (2001). With the initial value f_0 representing the rubber content in ABS, the porosity may increase in the course of deformation due to void growth in the plastically incompressible SAN matrix. Hence, macroscopic yielding of the porous material will involve plastic dilatancy under hydrostatic stress.

Gurson (1977) derived a now well-known yield function for porous, rigid perfectly plastic matrix materials, which involves an exponential dependence on hydrostatic stress. Since then, a number of extensions have been suggested in the literature accounting for more general material behavior. Paying special attention to the effect of non-negligible elastic strains around growing voids in a glassy polymer, Steenbrink et al. (1998) and Pijnenburg and Van der Giessen (2001) developed such a model showing much better agreement with cell calculations than the unmodified Gurson model. However, in view of the complexity of this model and of the error made in approximating the cavitated rubber particles as voids, we adopt here an alternative and computationally more convenient approach.

We assume the phenomenological macroscopic yield function

$$\Phi \equiv \frac{1}{2}\bar{\boldsymbol{\sigma}}' \cdot \bar{\boldsymbol{\sigma}}' + a f_0^b \sigma_{\mathrm{m}}^2 - [(1-f)\tau c(f_0)]^2 = 0, \tag{6}$$

which in contrast to the Gurson model exhibits only a quadratic dependence on hydrostatic stress. The 'pressure sensitivity' parameters a and b express the influence of hydrostatic (mean) stress σ_{m} and will be fitted from calculations with a RVE of voided SAN. The equivalent driving stress τ in the SAN matrix phase due to the stress state $\boldsymbol{\sigma}$ acting on the porous material is determined from the condition $\Phi = 0$.

Because of the intrinsic softening of SAN, plastic flow at the onset of macroscopic yield is not uniform throughout the matrix phase but localizes in the ligament connecting neighboring voids (Pijnenburg et al., 1999; Pijnenburg and Van der Giessen, 2001). Therefore the driving stress of the porous material should (at least initially, i.e. for $f = f_0$) scale with the relative width (area fraction) of the ligament between voids rather than with the volume fraction $1 - f$ of the matrix. To account for this heterogeneous plastic flow, the factor $c(f_0)$ depending on the initial porosity is introduced such that $(1 - f)\tau c(f_0)$ can be regarded as the equivalent driving stress of the porous material. For example, choosing $c(f_0) = (1 + \sqrt{f_0})^{-1}$ for the 2D case of cylindrical voids, the equivalent driving stress for $f = f_0$ becomes $(1 - \sqrt{f_0})\tau$ where $1 - \sqrt{f_0}$ is approximately the relative width of the ligament between voids in a square array (Pijnenburg and Van der Giessen, 2001).

The plastic strain rate is determined via the (normality) flow rule

$$\boldsymbol{D}^{\mathrm{p}} = \Lambda \frac{\partial \Phi}{\partial \bar{\boldsymbol{\sigma}}}, \tag{7}$$

where the multiplier Λ is computed from the condition that the plastic work rate per unit deformed volume of the porous material equals the dissipation in the matrix:

$$\bar{\boldsymbol{\sigma}} \cdot \boldsymbol{D}^{\mathrm{p}} = (1 - f)\sqrt{2}\tau\dot{\gamma}^{\mathrm{p}}. \tag{8}$$

With the equivalent driving stress τ in the matrix determined from (6), the equivalent plastic strain rate $\dot{\gamma}^{\mathrm{p}}$ obtained from (3) now represents the 'effective' visco-plastic behavior of the whole matrix phase. It differs from the equivalent plastic strain rate of the porous medium $\dot{\bar{\gamma}}^{\mathrm{p}} = \sqrt{\boldsymbol{D}^{\mathrm{p}} \cdot \boldsymbol{D}^{\mathrm{p}}}$ which also incorporates the effect of void growth. Due to the highly heterogeneous plastic flow in a porous glassy polymer the intrinsic softening of the matrix is evened out in the overall response (Smit et al., 1999). To incorporate this effect in the homogenized model, intrinsic softening is taken to decrease with increasing porosity. Not accounted for in the present treatment is the effect of porosity on the hardening behavior. The hardening modulus C_R and the limit stretch $\lambda_{\max}$ of SAN are taken to be valid also for ABS. In a more realistic model these quantities should also be replaced by 'effective' ones reflecting the heterogeneous and localized matrix stretching in ABS. Furthermore, the back stress tensor, being purely deviatoric for a plastically incompressible material, should have a volumetric component in a more consistent model for a porous material. However, numerical studies of void growth in glassy polymers have shown that matrix hardening has a negligible influence on the overall hydrostatic stress response since it affects only a thin shell-like region at the void surface (Steenbrink and Van der Giessen, 1997).

The numerical treatment in the present work follows exactly the method described in detail by Wu and Van der Giessen (1996) and employs a Total Lagrangian formulation of the finite deformation boundary value problem and a rate tangent integration of the constitutive equations. The latter is based on a method developed by Pierce et al. (1984) which also covers the case of plastically dilatant materials. When applied to the present ABS model the rate tangent formulation simplifies somewhat against the general procedure in Pierce et al. (1984) because of the special yield function (6). By rewriting (6) in terms of the weighted Cauchy stress $\boldsymbol{\sigma} \det \boldsymbol{F}$ where $\det \boldsymbol{F} = (1 - f_0)/(1 - f)$ because of the plastic incompressibility of the matrix in the ABS model, the current porosity f does not appear anymore. The weighted Cauchy stress tensor on the other hand is convenient for the Total Lagrangian formulation because of the correspondence of its components in convected coordinates to those of the second Piola–Kirchhoff stress tensor with respect to undeformed base vectors.

The determination of the 'free' parameters a and b in the macroscopic yield function (6) and its validation are based on 2D plane strain simulations with a block of voided SAN considered a RVE of the material. The block with the finite element discretization depicted in Fig. 3a contains 16 randomly located voids of initially equal size. Loading in terms of a uniform macroscopic deformation is specified by appropriately prescribing the velocities on the boundary of the block. Simulations under macroscopic equi-

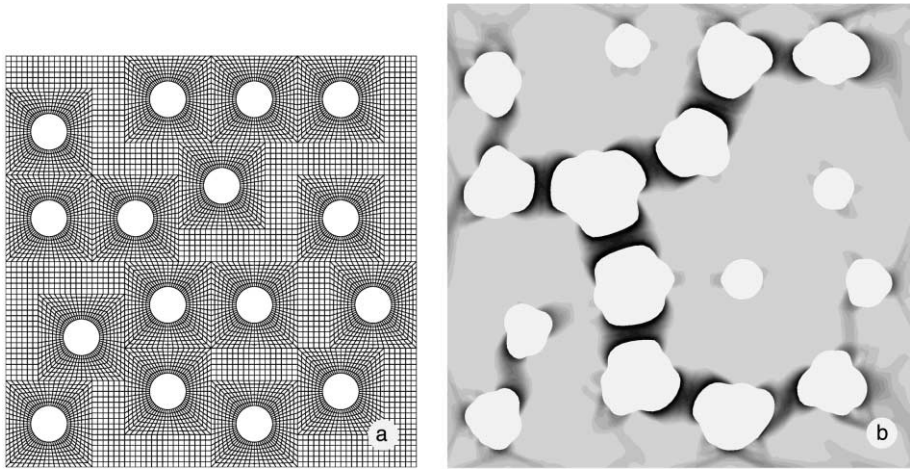

Fig. 3. Block of porous SAN employed for parameter fit in homogenized ABS model; (a) finite element mesh with void volume fraction $f_0 = 0.1$, (b) equi-biaxially deformed block at $E_V = 0.2$ with contours of accumulated plastic strain γ^p.

biaxial deformation for two different porosities serve to fit the 'pressure sensitivity' parameters to $a = 1$ and $b = 0.7$. The resulting response of the homogeneous ABS model in comparison to the overall response of the block is shown in Fig. 4 in terms of macroscopic mean Cauchy stress Σ_m versus macroscopic volumetric strain $E_V = E_1 + E_2$. Also depicted are results for a periodic void arrangement, represented by a single void unit cell. The softer post-yield response of the random void arrangement is due to the percolation of localized shearing and necking in between voids throughout the block, which is excluded in the unit cell model. To illustrate this phenomenon, Fig. 3b shows the deformed block at $E_V = 0.2$ with localized zones of highly enlarged voids and contours of accumulated plastic strain (dark). The dependence of the macroscopic response on the chosen RVE is a general problem in the homogenization of materials with

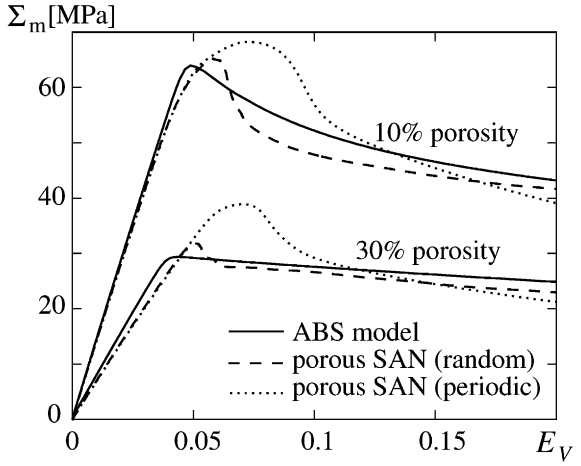

Fig. 4. True stress versus logarithmic strain response of the ABS model and porous SAN with random and periodic void arrangement under macroscopic equi-biaxial deformation.

microscale instabilities (intrinsic matrix softening and void growth in the present case). We have chosen the softer (less constrained) response to fit the effective homogeneous material model for ABS to be used in the PC/ABS blend model (Section 2).

With the parameters a and b fixed, Fig. 5 compares yield surfaces in Σ_e–Σ_m space obtained from (6) with those predicted by Pijnenburg and Van der Giessen (2001) using a modified Gurson model. In view of the simplicity of the present model the agreement is quite satisfactory. To further validate the ABS model its response is checked against the overall response of porous SAN with a random and a periodic void arrangement under macroscopic simple shear and uniaxial strain (Fig. 6). For values of the porosity in the relevant range the homogenized ABS model captures the elastic stiffness, the yield point, as well as the post-yield behavior of a porous glassy polymer to an acceptable degree of accuracy. Also shown in Fig. 6a is the response of neat SAN, i.e. ABS with 0% rubber content (porosity).

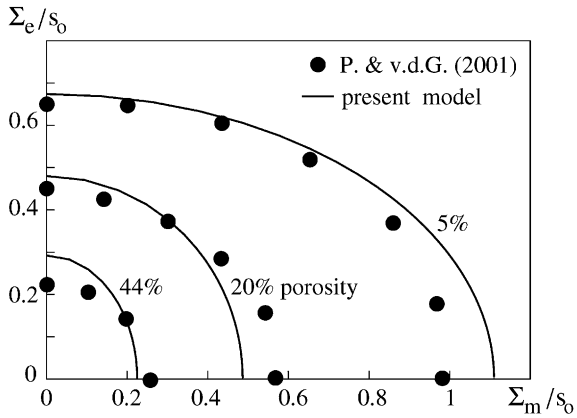

Fig. 5. Yield surfaces computed from (6) (normalized by the initial yield strength of SAN) compared to data obtained from modified Gurson yield function (Pijnenburg and Van der Giessen, 2001).

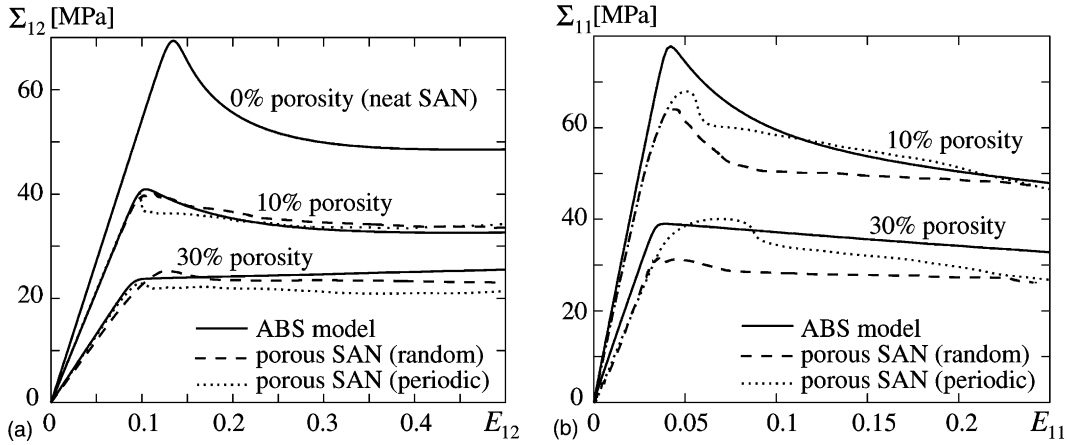

Fig. 6. Validation of ABS model in comparison to macroscopic response of porous SAN: (a) simple shear and (b) uniaxial strain.

4. Results—PC/ABS blends

The investigation of PC/ABS blends is performed for the periodic arrays of ABS particles embedded in a PC matrix as depicted in Fig. 2. The main parameters characterizing the blends are the volume fraction of ABS as the so-called modifier phase, and the rubber content in ABS represented by the porosity in the effective ABS model. Particulate microstructures with approximately spherical ABS particles are found in real blends for volume fractions of up to 40%, and the rubber content in commercial ABS ranges from 10% to 40% (e.g. Ishikawa, 1995; Greco, 1996; Inberg, 2001). In view of the fact that in real ABS not all rubber particles cavitate and those having cavitated still carry some load, in a model treating them as voids the porosity should be taken somewhat smaller than the true rubber content.

The overall response of various blends is illustrated in Fig. 7 in terms of the principal macroscopic stress Σ_1 versus the macroscopic logarithmic strain E_1. By specifying the macroscopic deformation to uniaxial strain ($E_2 = 0$) a volumetric expansion of the blend is enforced. This leads to high stresses and no softening in neat PC and the blend of PC with 25% SAN, since both are plastically incompressible. In contrast, the PC/ABS blends allow for macroscopic volumetric yielding which causes the macro stress response to plateau out. At a fixed rubber content of 15% in ABS, this plateau stress is seen to be hardly affected by the amount of ABS in the blend, whereas at a fixed ABS volume fraction (25%) the macroscopic flow stress level strongly depends on the rubber content (porosity) in ABS. This dependence is obvious from the overall stiffness of the blend decreasing with increasing rubber content in the modifier phase. The extreme case of no rubber is represented by the PC/SAN blend, while porous PC can be regarded as the limit of very high (100%) porosity in ABS. The different response of the blends under the same overall deformation is also reflected in the macroscopic stress triaxiality $T_\Sigma = \Sigma_m/\Sigma_e$. At a macroscopic strain of $E_1 = 0.25$ its values are: $T_\Sigma \approx 3$ for the two blends (25% and 40% ABS) with 15% rubber in the ABS and for porous PC (25% porosity); $T_\Sigma \approx 4$ for the ABS type with 5% rubber; $T_\Sigma \approx 6$ for neat PC; and $T_\Sigma \approx 10$ for the PC/SAN blend. The macroscopic mean stress Σ_m (not shown here for brevity) displays a similar behavior as that in Fig. 7. This does not change qualitatively for other ratios of macroscopic strain E_2/E_1 that enforce overall volumetric expansion which is to be accommodated by plastic dilatation of the ABS. It should be noted that by keeping the macroscopic strain ratio E_2/E_1 constant, the present analyzes are different from earlier ones

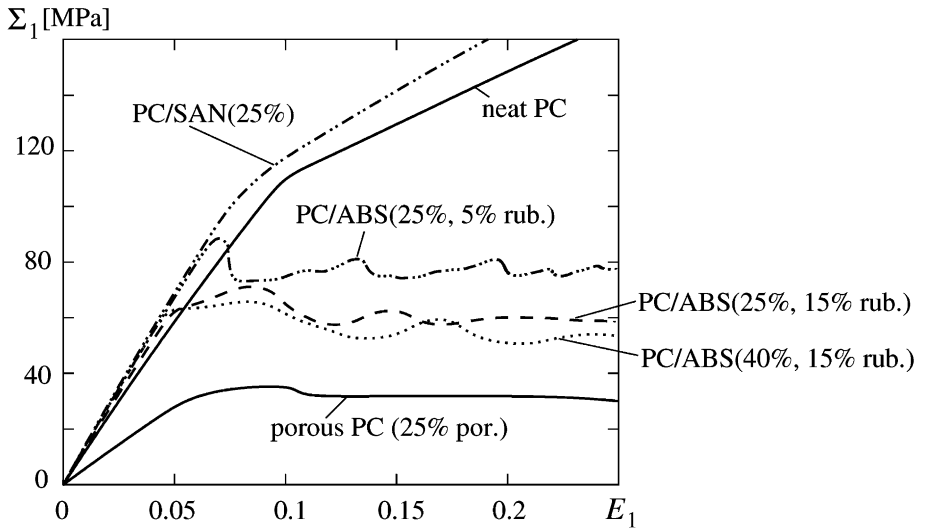

Fig. 7. Macroscopic response of blends under uniaxial overall strain E_1.

(e.g. Steenbrink et al., 1998; Socrate and Boyce, 2000) where one component of macrostrain is adjusted to keep T_Σ constant. However, it is not clear which way of loading is more realistic and more suited for extracting information from the response of the blends.

4.1. Patterns of localized plastic deformation

Localization of plastic deformation in homogeneous, plastically incompressible glassy polymers (PC, SAN) takes place by shear banding and results from the intrinsic softening of these materials. In ABS, modeled as a porous material, another type of 'material' instability comes into play by void growth (on the microscale) and this may lead to the localization of volumetric yielding. Because of the interaction of these two types of instabilities the patterns of localized plastic deformation in PC/ABS blends are expected to be more complex than in merely porous plastics ('binary' blends). They may depend on the constituent properties, the blend morphology and the 'mode' of overall deformation imposed on the blend.

4.1.1. Effect of modifier type and morphology

Fig. 8 summarizes how localization of plastic deformation in polymer blends may depend on the morphology and qualitatively different modifier types. Blends with a PC matrix and a 25% volume fraction of either ABS particles, SAN particles or voids are compared for square and hexagonal microstructures. A rubber content (porosity) of 15% is chosen for the ABS. SAN and voids can be taken as extreme cases of ABS with a rubber content of 0% or 100%, respectively. The macroscopic deformation is specified by a ratio of principal strains of $E_2/E_1 = -0.43$ where E_1 is the horizontal component (Fig. 8). For neat PC this mode of deformation would correspond to a state of uniaxial tension in the elastic range. Plastic deformation is visualized in Fig. 8 in terms of the accumulated plastic strain $\tilde{\gamma}^{\mathrm{p}}$ at an overall deformation of $E_1 = 0.16$. Shear bands in the PC matrix form at an angle of $\approx 45^\circ$ (corresponding to the direction of maximum macroscopic shear stress) for all blends except for the square void arrangement where yielding takes place by necking of the intervoid ligament perpendicular to the overall straining direction (Fig. 8c). The latter observation for voided PC has also been made by Socrate and Boyce (2000). Shear bands in the PC/ABS blends connect neighboring ABS particles and are continued inside the particles by localized zones of essentially volumetric yielding.

As will be discussed in more detail in Section 4.1.2, the matrix shear bands in the hexagonal blend (Fig. 8b) originate from the ABS particles after the zones of plastic dilatation inside have formed and then spread into the matrix. This explains the occurrence of two parallel shear bands between each pair of particles. A similar pattern can be seen in case of the hexagonal void arrangement (Fig. 8d). Shear bands connecting neighboring modifier particles will later on (Section 4.1.3) be identified as being beneficial for toughening (by lowering peak values of hydrostatic stress in the PC matrix). Comparing Fig. 8a and c shows that this is more likely to be accomplished by adding ABS rather than by adding voids. Shear bands in PC/SAN blends (Fig. 8e and f) form tangential to the stiff and plastically non-dilatant SAN particles and do not 'directly' connect neighboring particles. Plastic deformation in the PC matrix then is more diffuse (than in case of ABS particles or voids) due to the formation of secondary shear bands originating from intersection points of the primary (dark) ones. At the instant shown in Fig. 8 no yielding has taken place in the SAN phase.

4.1.2. Effect of rubber content

Experiments indicate that the toughening effect of blending PC with ABS strongly depends on the ABS type (Greco, 1996). One possible source of this dependence, amongst other parameters involved, is the rubber content. Here we will show that already the way in which plastic deformation localizes in the blend may differ qualitatively with the rubber content; its effect on toughening will be analyzed in Section 4.2. In terms of the equivalent plastic strain rate $\dot{\tilde{\gamma}}^{\mathrm{p}}$, Fig. 9 gives an instantaneous picture of the spreading of localized plastic flow at two stages ($E_1 = 0.1, 0.16$) in the course of overall uniaxial straining ($E_2 = 0$) of two

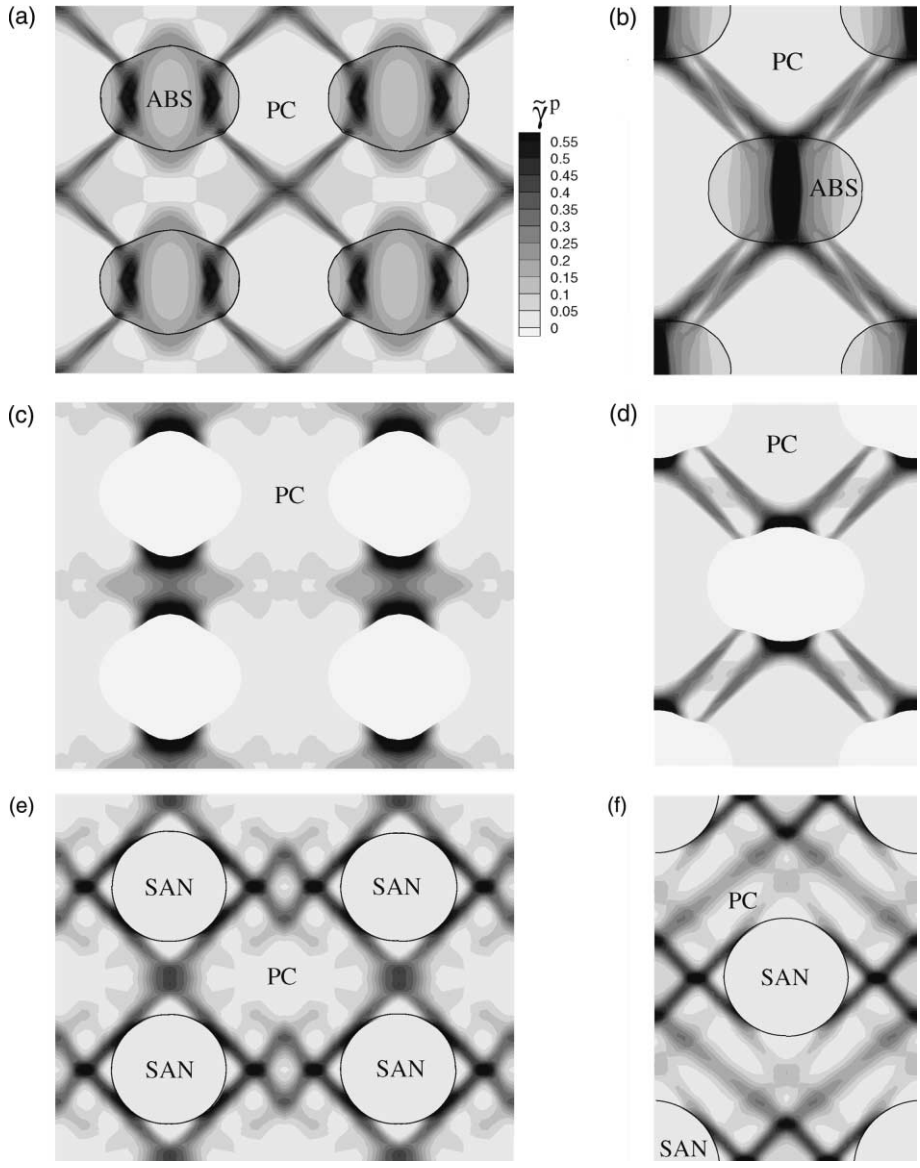

Fig. 8. Patterns of localized plastic deformation in blends with square (left) and hexagonal (right) microstructure and 25% ABS, SAN or voids as the modifier phase; the level of macroscopic deformation is $E_1 = 0.16$.

different blends. The blends differ in terms of the rubber content in ABS, which is either 15% (Fig. 9a) or 5% (Fig. 9b). In case of the higher rubber content (i.e. softer ABS), yielding first localizes in a narrow zone inside the ABS particles perpendicular to the (horizontal) straining direction. Shear bands in the PC matrix originate from these zones in the 'equator region' of the particles ($E_1 = 0.1$) and later link up with those terminating from neighboring particles ($E_1 = 0.16$). The resulting shear band pattern is similar to that seen in Fig. 8b. Plastic deformation in the stiffer ABS (lower rubber content, Fig. 9b) localizes along the interface to the matrix and does not reach the particles' equator region. With increasing overall deformation

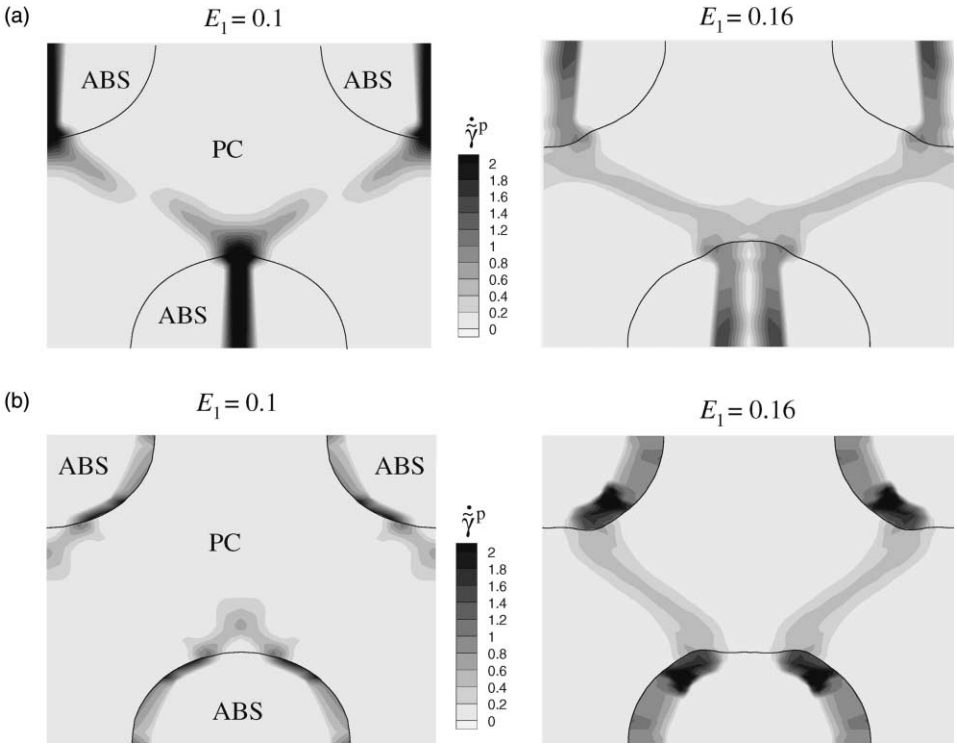

Fig. 9. Evolution of localized plastic deformation in PC/ABS blends under uniaxial horizontal strain E_1. The rubber content in ABS is (a) 15% and (b) 5%.

($E_1 = 0.16$) shear bands having a different orientation than those in Fig. 9a spread in the PC matrix and connect ABS particles while the small region of earlier matrix yielding ahead of the particle equator dies out.

It should be mentioned that the above phenomenon also depends on the 'mode' of overall deformation. Doing the same simulation at the more shear-like ratio of macrostrains $E_2/E_1 = -0.43$ led to final patterns of localized plastic deformation similar to that in Fig. 9a for both values of the rubber content. However, for the ABS particles with the lower rubber content, at initiation of plastic flow a competition could be noticed between localization in the equator region or localization in the interface.

4.1.3. Effect of straining direction versus particle arrangement

Though being elastically isotropic, PC/ABS blends with a hexagonal microstructure exhibit anisotropic yield with a significant effect on the pattern of localized plastic deformation and on the local stress distribution. This phenomenon is illustrated in Fig. 10 for a blend with 25% ABS particles containing 15% rubber, again subjected to uniaxial macroscopic strain. For particle rows parallel to the direction of overall straining, the angle between neighboring particles in adjacent rows and the straining direction is initially 60° (see Fig. 2a). A reduction of this angle towards the direction of principal macroscopic shear stress (45°) takes place in the course of overall (horizontal) straining and promotes the formation of shear bands bridging the matrix ligament between adjacent particle rows. This was the case in the previous example (Fig. 9a) and is shown again by the right-hand inset of Fig. 10. On the other hand, when the particle rows are perpendicular to the direction of overall straining the angle between particles in adjacent layers and the

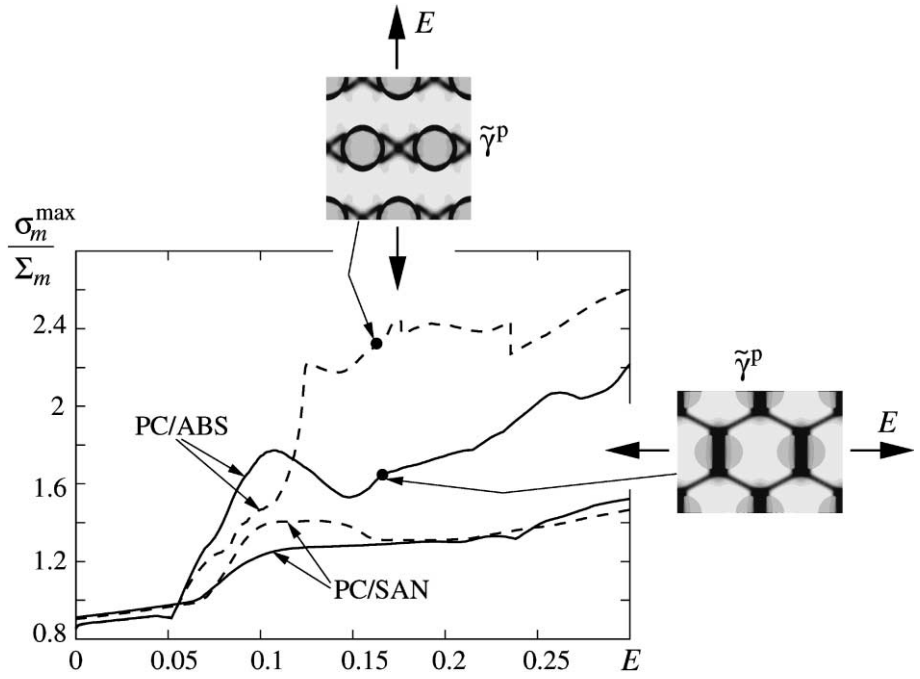

Fig. 10. Effect of overall straining direction with respect to hexagonal particle arrangement on pattern of localized plastic deformation and peak values of hydrostatic stress. Insets show distribution of accumulated plastic strain in PC/ABS blend at $E = 0.16$.

straining direction is initially 30° (Fig. 2a) and further decreases due to the overall deformation. Matrix shear banding then takes place only between particles of the same rows and shows a crossing pattern as visualized by the upper inset in Fig. 10. In this case plastic deformation inside the particles is localized along the PC/ABS interface.

Whether or not a network of shear bands between particles forms throughout the microstructure has a strong influence on the local stress distribution. Normalized by the macroscopic hydrostatic stress Σ_m, the peak values of hydrostatic stress in the PC matrix, σ_m^{max}/Σ_m, versus macroscopic strain are shown in Fig. 10. For comparison also the response of PC/SAN blends is depicted. In the case of PC/ABS blends, localization of plastic flow in a hexagonal pattern as in the right-hand inset gives rise to significantly lower values of σ_m^{max}/Σ_m. This difference partly results from the softer overall response and hence lower Σ_m values in case of the soft 'layers' of intense plastic flow formed perpendicular to the straining direction in the upper inset. Another reason is the crossing of shear bands, which leads to locally high σ_m values near the intersection of the bands. Hydrostatic stresses in PC/SAN blends where the modifier particles do not allow for volumetric yielding are much higher than in PC/ABS but a more uniform stress distribution leads to lower values of σ_m^{max}/Σ_m with a minor dependence on the morphology (Fig. 10).

The distinction of morphologies made here in terms of their orientation might seem irrelevant with regard to real blends with a random microstructure. But, the results obtained lead us to conclude that the formation of a network of matrix shear bands connecting modifier particles is beneficial for reducing peak hydrostatic stresses and therefore contributes to toughening. Since such a 'morphological effect' is not displayed by the response of PC/SAN blends (Fig. 10) it may further be concluded that this preferred type of matrix shear banding is promoted by the plastic dilatancy shown by ABS in contrast to SAN, provided that the overall deformation is not too much constrained. This idea is also supported by the results of Fig. 8. Furthermore, comparison of the effect of voids (Fig. 8c) and ABS particles (Fig. 8a)—both showing

dilatancy but not necessarily shear banding—indicates that toughening via matrix shear banding requires the right proportion between plastic dilatancy and stiffness of the modifier particles.

4.2. Toughening implications

The superior fracture toughness of PC/ABS blends compared to that of homogeneous PC is generally understood to result from an enhanced energy absorption and a suppression or delay of crazing. Craze initiation in the PC matrix as a precursor of brittle failure is primarily determined by hydrostatic stress. Therefore, the overall dissipated work $W_{\mathrm{diss}} = \int_0^t \int_V \bar{\boldsymbol{\sigma}} \cdot \boldsymbol{D}^{\mathrm{p}} \, \mathrm{d}V \, \mathrm{d}t$ and the peak value $\sigma_{\mathrm{m}}^{\max}$ of hydrostatic (mean) stress anywhere in the PC matrix are considered here as global and local indicators allowing a qualitative insight into how the toughness may depend on characteristics of the blend. PC/ABS blends are compared for various values of the ABS content in the blend and of the rubber content in ABS. Computations are carried out for a hexagonal microstructure under uniaxial macroscopic strain E_1 (orientation as in Fig. 10, right-hand inset).

4.2.1. Influence of ABS volume fraction in the blend

For a fixed ABS type with a typical rubber content of 15%, Fig. 11a and b shows the dissipated work versus macroscopic strain for blends with an ABS volume fraction of 0% (neat PC), 10%, 25%, 40% and 100% (neat ABS). The absolute dissipated work $\overline{W}_{\mathrm{diss}}$ (per unit initial volume V_0 of the blend as indicated by the bar) clearly exceeds the value for neat PC as soon as ABS is present in the blend while the amount of ABS is of minor influence (Fig. 11a). The dependence on the ABS content becomes quite pronounced when the dissipated work is related to the total energy W_{tot} put into the material. Fig. 11b shows that $W_{\mathrm{diss}}/W_{\mathrm{tot}}$, i.e. the percentage of work dissipated, increases monotonically with the ABS content in the blend. This can be explained from a large contribution of volumetric yielding in ABS to the overall dissipation in the present case of enforced macroscopic dilatation (uniaxial strain, $E_2 = 0$). In case of neat PC which is plastically incompressible $W_{\mathrm{diss}}/W_{\mathrm{tot}}$ is much lower and after attaining a maximum decreases with increasing strain (Fig. 11b). The enhanced energy absorption in PC/ABS blends is thus understood to be one reason for the higher toughness. At the same time the hydrostatic stress in neat PC rises linearly to rather high values (Fig. 11c) whereas in the PC/ABS blends its peak values tend to a plateau of around 100 MPa. This significant reduction of peak hydrostatic stresses in the PC matrix compared to those in neat PC is due to volumetric expansion in ABS accommodating the prescribed overall deformation. It can be interpreted as a further toughening effect reducing the propensity for crazing. As displayed in Fig. 11c the absolute values $\sigma_{\mathrm{m}}^{\max}$ are slightly lowered by increasing the amount of ABS in the blend.

To address the issue of an optimal ABS content ('synergistic effect') in the range of 20–30% reported in experiments by Greco et al. (1994), numerical values of our various 'toughening indicators' are collectively shown in Fig. 11d as functions of the ABS content in the blend. The presented values are those attained at a macroscopic strain of $E_1 = 0.32$. They are normalized by the respective values obtained for neat PC (0% ABS), and the curve showing the dissipated work compared to the stored elastic energy W_{el} has been rescaled by a factor of 5. The elastically stored energy may become important in a fracture process when it is released during unloading in the wake of the crack. When related to the macroscopic stress state, the peak value of hydrostatic stress $\sigma_{\mathrm{m}}^{\max}/\Sigma_{\mathrm{m}}$ of course exceeds the value 1 for neat PC where the stress distribution is uniform. However, $\sigma_{\mathrm{m}}^{\max}/\Sigma_{\mathrm{m}}$ seems to level off for an ABS content above 25% which means that the propensity for crazing does not increase further with the ABS content even under the same macroscopic stress. In contrast, both $W_{\mathrm{diss}}/W_{\mathrm{tot}}$ and $W_{\mathrm{diss}}/W_{\mathrm{el}}$ monotonically increase with the ABS volume fraction (see also Fig. 11b). Combining the behavior of these quantities leads to the interpretation that the more ABS contained in the blend the tougher the material is. Thus, a maximum toughness of the blend in the intermediate range of ABS content mentioned above cannot be concluded from the present study. This discrepancy with experimental findings may be attributed to a transition in the morphology as well as in the failure mechanisms

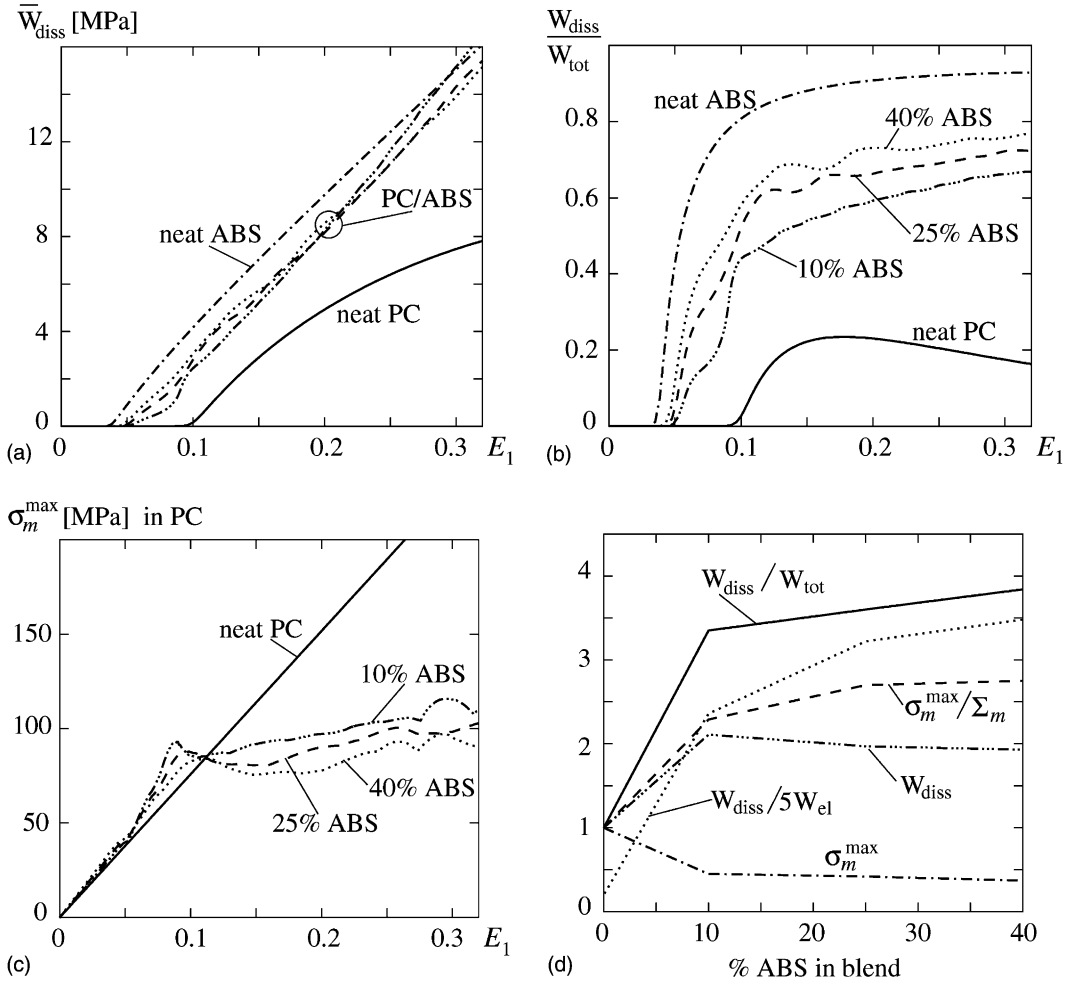

Fig. 11. Effect of ABS volume fraction in blend (15% rubber content in ABS): (a) work dissipated per volume of the blend, (b) dissipated work per total work, (c) peak values of hydrostatic stress in PC matrix, (d) data versus ABS content at macrostrain $E_1 = 0.32$ (normalized by values for neat PC).

observed in real blends for increasing ABS content (Inberg, 2001), both of which are not accounted for in the present model.

4.2.2. Influence of rubber content in ABS

To investigate the influence of the ABS type on the performance of PC/ABS blends, the rubber content in ABS (porosity) is varied from 0% to 35% while the volume fraction of ABS in the blend is now kept fixed at 25%. The same 'toughening indicators' as before are given in Fig. 12 where for comparison also the data for unmodified (neat) PC are included. A remarkable result is that the dependence of energy dissipation on the rubber content is 'opposite' to its dependence on the ABS volume fraction. In contrast to Fig. 11a and b, here the absolute dissipated work $\overline{W}_{diss}$ shows a significant dependence on the rubber content in ABS (Fig. 12a) whereas the percentage of work dissipated W_{diss}/W_{tot} is hardly affected as soon as the ABS contains some amount of rubber (Fig. 12b). For the PC/SAN blend (0% rubber) $\overline{W}_{diss}$ and W_{diss}/W_{tot} are

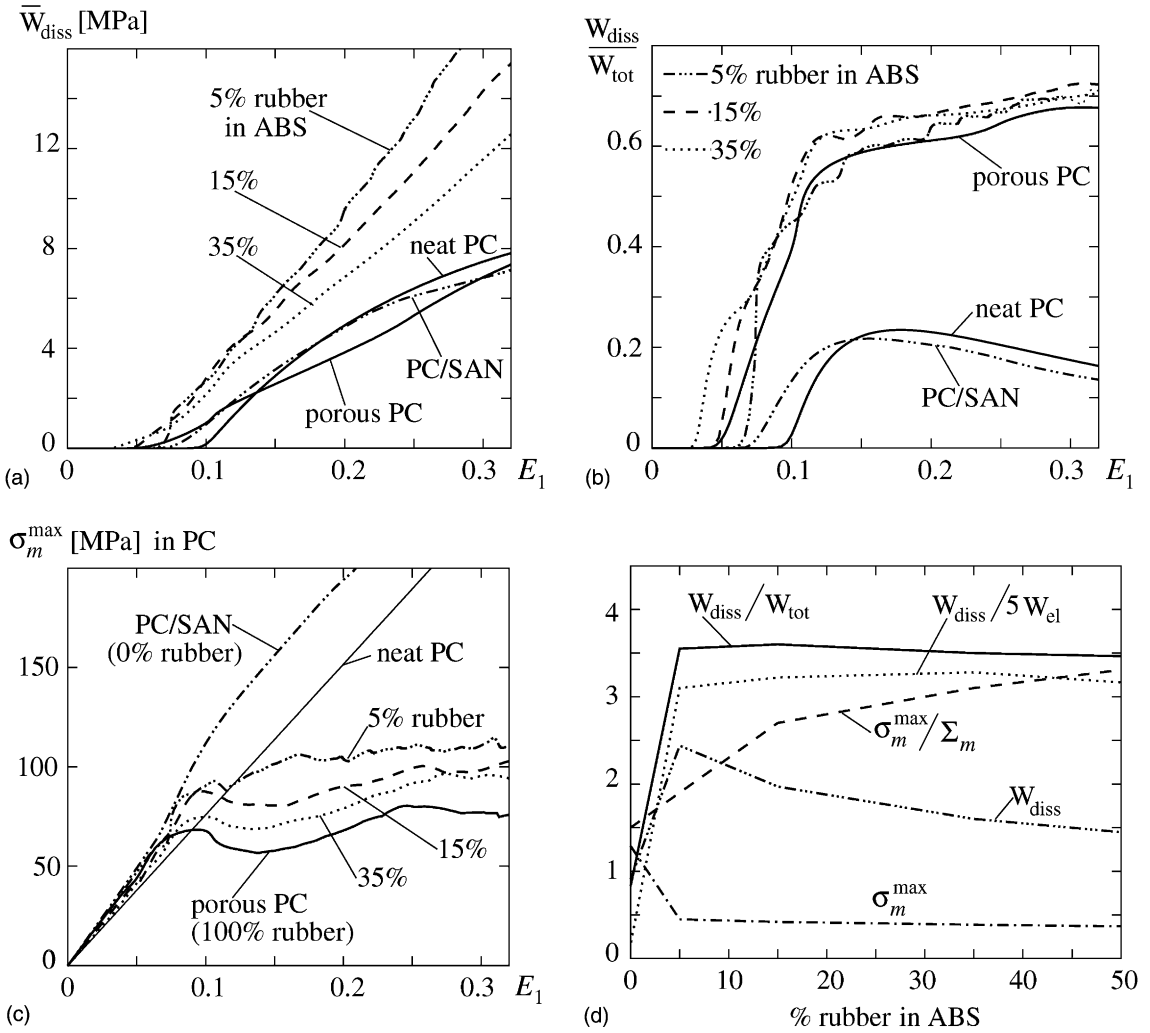

Fig. 12. Effect of rubber content in ABS (25% ABS in blend): (a) work dissipated per volume of the blend, (b) dissipated work per total work, (c) peak values of hydrostatic stress in PC matrix, (d) data versus rubber content at macrostrain $E_1 = 0.32$ (normalized by values for neat PC).

approximately the same as for neat PC and much lower than for the PC/ABS blends, which again can be taken as an indication for toughening by ABS. The important contribution of ABS to the energy dissipation can also be seen from the behavior of porous PC for which the absolute dissipation $\overline{W}_{diss}$ is as low as for neat PC (Fig. 12a). The observation that porous PC reaches the same level of dissipation as the PC/ABS blends in terms of W_{diss}/W_{tot} (Fig. 12b) can be explained from the softer overall response of porous PC leading to lower values of W_{tot} under the same macroscopic deformation. It seems interesting to note that the higher overall stiffness (see also Fig. 7) and hence W_{tot} of the blend containing ABS with 5% rubber does not lead to a lower value of W_{diss}/W_{tot} which in correspondence to Fig. 12a indicates that ABS with a low rubber content makes the blend more dissipative. In case of PC/ABS blends the peak hydrostatic stresses σ_m^{max} in the PC matrix shown in Fig. 12c tend to plateau-like values after the onset of yielding which de-

crease with increasing rubber content in ABS. Without the ability for macroscopic volumetric yielding (PC/SAN) enabled by cavitation of rubber particles, σ_m^{max} values are even higher than in neat PC.

Values of the different measures of hydrostatic stress and dissipation at macroscopic strain $E_1 = 0.32$ are summarized in Fig. 12d versus the rubber content in ABS. Again all quantities are normalized by the respective values for neat PC. The absorbed energy as well as its ratios to the total work and to the elastically stored energy show maxima in the range of 5–35% rubber content. On the other hand, the monotonic increase of σ_m^{max}/Σ_m indicates an increasing propensity for matrix crazing with increasing rubber content in ABS for sufficiently high overall hydrostatic stress. Therefore, it might be concluded—at least in the framework of the present model—that PC/ABS blends show an optimal toughness for ABS with a rubber content in the range between 5% and 35%.

5. Conclusion

Patterns of localized plastic deformation in polymer blends of PC/ABS have been investigated with respect to their dependence on microstructural features such as blend composition and phase properties. The blend model is based on the simplifying assumption that ABS which is itself a heterogeneous material, can be represented by a homogenized material. The effective ABS behavior then is that of a porous glassy polymer where plastic dilatancy corresponds to void growth in the SAN matrix of real ABS initiated by rubber particle cavitation. Intrinsic shear softening in PC and volumetric softening in ABS both lead to material instabilities which interact via the blend microstructure. This interaction has been shown to promote the formation of shear bands in the PC matrix which terminate from zones of localized yielding in the ABS particles and connect neighboring particles.

The study was motivated by the interest in the micromechanisms contributing to the fracture toughness of polymer blends which is generally understood to result from the competition of energy absorption and brittle failure by crazing. With regard to crazing, which is primarily governed by hydrostatic stress, the simulations reveal that a network-like pattern of localized plastic deformations throughout the microstructure is beneficial for reducing peak values of hydrostatic stress. This together with an enhanced energy dissipation emphasizes the key role played by localized plastic deformations for toughening of PC.

The rubber content is known to be an important parameter determining (among others) the suitability of ABS as a toughening modifier. Its effect has been explored by varying the porosity in the blend model, and has been seen to lead to significant differences in the plastic flow localization in the ABS phase with an impact on the shear band pattern in the PC matrix (Fig. 9). The investigation of the influence of rubber content on overall energy dissipation and peak hydrostatic stress as indicators for toughening, suggests an optimal range of rubber content in ABS. An optimal range for the ABS content, as reported in the experimental literature (at least for some ABS types), could not be identified in the present study. In fact, the results indicate an increasing toughness with increasing ABS content.

This discrepancy of course has to be seen in the light of the simplifying assumptions made in the present model compared to real fracture in real materials. The geometry of the blend model with 2D unit cells and special loading conditions is evidently a rather simple one compared to those applied to binary blends, e.g. by Smit et al. (1999) or Socrate and Boyce (2000). However, as a first step in the analysis of ternary blends incorporating effects such as energy absorption and plastic dilatancy in the modifier phase, this simplification seems acceptable in view of further uncertainties in the model. Since the relative size of ABS and rubber particles is in the range of 10–20 (Greco, 1996; Inberg, 2001), the number of rubber particles (voids) in a typical ABS particle is not very large. Therefore, and because of the percolation of localized plastic flow (see Fig. 3b), it is not clear what the effect is of having homogenized the ABS phase. Moreover, toughness measurements involve propagation of a crack with a 'tip radius' much smaller than the initial notch in

Fig. 1. Loading of the blend material then is highly non-uniform, and the absolute particle size introduces a characteristic length scale to the problem.

References

Arruda, E.M., Boyce, M.C., 1993. A three-dimensional constitutive model for the large stretch behavior of rubber elastic materials. Journal of the Mechanics and Physics of Solids 41, 389–412.

Boyce, M.C., Parks, D.M., Argon, A.S., 1988. Large inelastic deformation of glassy polymers. Mechanics of Materials 7, 15–33.

Bucknall, C.B., 1997. Rubber toughening. In: The Physics of Glassy Polymers. Chapman & Hall, London, pp. 363–412.

Donald, A.M., 1997. Crazing. In: The Physics of Glassy Polymers. Chapman & Hall, London, pp. 295–341.

G'Sell, C., Hiver, J.M., Dahoun, A., Souahi, A., 1992. Video-controlled tensile testing of polymers and metals beyond the necking point. Journal of Materials Science 27, 5031–5039.

Greco, R., Astarita, M.F., Dong, L., Sorrentino, A., 1994. Polycarbonate/ABS blends: processability, thermal properties, and mechanical and impact behavior. Advances in Polymer Technology 13 (4), 259–274.

Greco, R., 1996. Polycarbonate toughening by ABS. In: Advanced Routes for Polymer Toughening. Elsevier, Amsterdam, pp. 469–526.

Gurson, A.L., 1977. Continuum theory of ductile rupture by void nucleation and growth. Journal of Engineering Materials and Technology 99, 2–15.

Inberg, J.P.F., 2001. Fracture of polycarbonate/ABS blends. PhD thesis, University of Twente, Enschede, The Netherlands.

Ishikawa, M., 1995. Stability of plastic deformation and toughness of polycarbonate blended with poly(acrylonitrile–butadiene–styrene) copolymer. Polymer 36 (11), 2203–2210.

Pierce, D., Shih, C.F., Needleman, A., 1984. A tangent modulus method for rate dependent solids. Computers and Structures 18, 875–887.

Pijnenburg, K.G.W., Steenbrink, A.C., Van der Giessen, E., 1999. Shearing of particles during crack growth in polymer blends. Polymer 40, 5761–5771.

Pijnenburg, K.G.W., Van der Giessen, E., 2001. Macroscopic yield in cavitated polymer blends. International Journal of Solids and Structures 38, 3575–3598.

Smit, R.J.M., Brekelmans, W.A.M., Meijer, H.E.H., 1999. Prediction of the large-strain mechanical response of heterogeneous polymer systems: local and global deformation behavior of a representative volume element of voided polycarbonate. Journal of the Mechanics and Physics of Solids 47, 201–221.

Socrate, S., Boyce, M.C., 2000. Micromechanics of toughened polycarbonate. Journal of the Mechanics and Physics of Solids 48, 233–273.

Steenbrink, A.C., Van der Giessen, E., 1997. Void growth in glassy polymers: effect of yield properties on hydrostatic expansion. International Journal of Damage Mechanics 6, 317–330.

Steenbrink, A.C., Van der Giessen, E., Wu, P.D., 1998. Studies on the growth of voids in amorphous glassy polymers. Journal of Materials Science 33, 3163–3175.

Steenbrink, A.C., Van der Giessen, E., 1999. On cavitation, post-cavitation and yield in amorphous polymer-rubber blends. Journal of the Mechanics and Physics of Solids 47, 843–876.

Wu, P.D., Van der Giessen, E., 1996. Computational aspects of localized deformations in amorphous glassy polymers. European Journal of Mechanics A 15 (5), 799–823.

Yee, A.F., 1977. The yield and deformation behaviour of some polycarbonate blends. Journal of Materials Science 12, 757–765.